Journal of Low Temperature Physics
https://doi.org/10.1007/s10909-024-03100-6

Results and Limits of Time-Division Multiplexing for the BICEP Array High-Frequency Receivers

S. Fatigoni · P. A. R. Ade · Z. Ahmed · M. Amiri · D. Barkats · R. Basu Thakur, et al. ***[full author details at the end of the article]***

Received: 24 October 2023 / Accepted: 1 April 2024

Abstract
Time-division multiplexing is the readout architecture of choice for many ground and space experiments, as it is a very mature technology with proven outstanding low-frequency noise stability, which represents a central challenge in multiplexing. Once fully populated, each of the two BICEP Array high-frequency receivers, observing at 150 GHz and 220/270 GHz, will have 7776 TES detectors tiled on the focal plane. The constraints set by these two receivers required a redesign of the warm readout electronics. The new version of the standard multichannel electronics, developed and built at the University of British Columbia, is presented here for the first time. BICEP Array operates time-division multiplexing readout technology to the limits of its capabilities in terms of multiplexing rate, noise and cross talk, and applies them in rigorously demanding scientific application requiring extreme noise performance and systematic error control. Future experiments like CMB-S4 plan to use TES bolometers with time-division/SQUID-based readout for an even larger number of detectors.

Keywords Time-division multiplexing · Readout electronics · Transition edge sensor · BICEP Array · Cosmology · Cosmic microwave background · B-mode polarization

1 Introduction

In the time-division multiplexing (TDM) readout scheme, each superconducting bolometer is inductively coupled to a SQUID amplifier. The detectors are grouped by rows and columns, and the signal is read out from all columns simultaneously, turning on one row at a time. Because the SQUID's response is intrinsically nonlinear, a feedback loop is used to calculate the correct flux to be sent to the SQUID feedback to compensate for changes in detector current and keep the amplification in a linear regime. This feedback current is also recorded as "signal." The multichannel electronics (MCE) system, developed and built at the University of British Columbia, supplies the bias current needed to keep the TES detectors in transition, controls

Published online: 24 April 2024

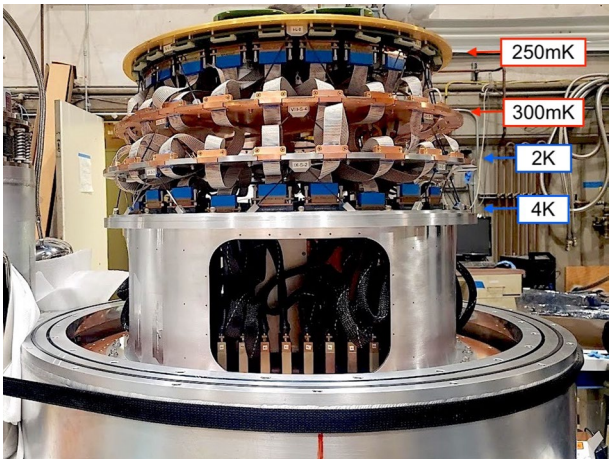

Fig. 1 Sub-Kelvin stages of the BICEP Array 150GHz cryostat, showing the high density of readout cables that must go from 0.25 K to 4 K with TDM readout. The same number of cables runs from 4K to 300K in the lower part of the cryostat not visible in this picture

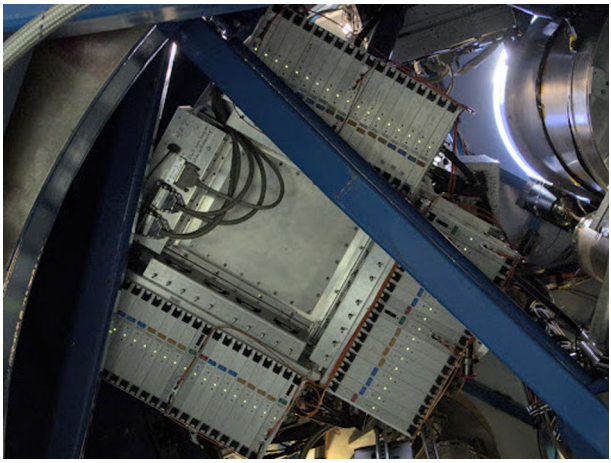

Fig. 2 Three double MCEs mounted on the deployed BICEP Array 150GHz receiver at the south pole

the multiplexer and SQUID amplifiers and reads the signal from a 41×32 element array [6, 9].

The total number of detectors that can be read out with TDM is limited by the thermal load induced by cables running from $250mK$ to $300K$ (Fig. 1), and the volume available to fit readout cables inside the cryostat and to fit warm electronics in the cryostat mount (Fig. 1). To address the latter problem, the BICEP Array (BA) two high-frequency receivers use a new version of the MCE, the double MCE (DMCE), that can read out a matrix of 41 rows x 64 columns [8]. Time-division multiplexing is the baseline technology for CMB-S4 [1, 5] (Fig. 2).

2 Detector Modules

The detector formats set up the requirements for the TDM readout electronics. The detectors used in BICEP Array are photon-noise-limited transition edge superconducting (TES) bolometers [4]. The pixel count in BA detector tiles is limited by the receiver frequency (see Table 1). The two BA high-frequency receivers, observing at 150GHz and 220/270GHz, share the same detector count and detector distribution on a tile, which is a 18x18 pixel tile, for a total of 324 pixels, or 648 detectors.

Detector tiles are included into a modular architecture which is shared between all the BA receivers [3]. Each module hosts SQUID chips for multiplexing, which interface with the detector tile through an interface PCB, to which they are individually wire-bonded. The number of wire bonds required is one of the challenging factors in using TDM for high-density pixel arrays (Fig. 3). All the SQUID chips (MUX and Nyquist) are made at NIST.

In 8 of the detectors in the matrix, the TES antenna is not connected, making these detectors sensitive to thermal drifts, RFI and direct island stimulation only. Two other pixels are occupied by loss test devices, where the incoming power is split equally between two paths, one of which has a lossy meander of known length. These two devices are used to estimate the signal loss through the feedline.

The detector module is composed of a layer stack that includes a quartz anti-reflection (AR) coating tile, the detector wafer, the $\lambda/4$ backshort, an A4K magnetic shield and two custom-designed PCBs. The module stack is housed in a superconducting niobium and aluminum box that together with a high-μ A4K sheet inside the module is designed to achieve high magnetic shielding performance [7]. The stack of layers inside each module is held together by custom-designed beryllium–copper clips that apply the right amount of pressure to hold the layers together.

Table 1 Detector count, MUX factor and readout electronics needed for each of the four BICEP Array receivers. Readout channels count for the three TDM BICEP Array receivers at 30/40, 95 and 150 GHz

Receiver Observing Band (GHz)	Number of Detectors per Module/Receiver	Mux Factor	MCE Type	Number of MCEs
30	32/192	33	*Single*	1
40	50/300	33	*Single*	
95	338/4,056	43	*Single*	3
150	648/7,776	41	*Double*	3
220	648/7,776	41	*Double*	3
270	648/7,776	41	*Double*	

BA1 30/40 GHz receiver is split in 2 colors counting each as a 0.5 MCE

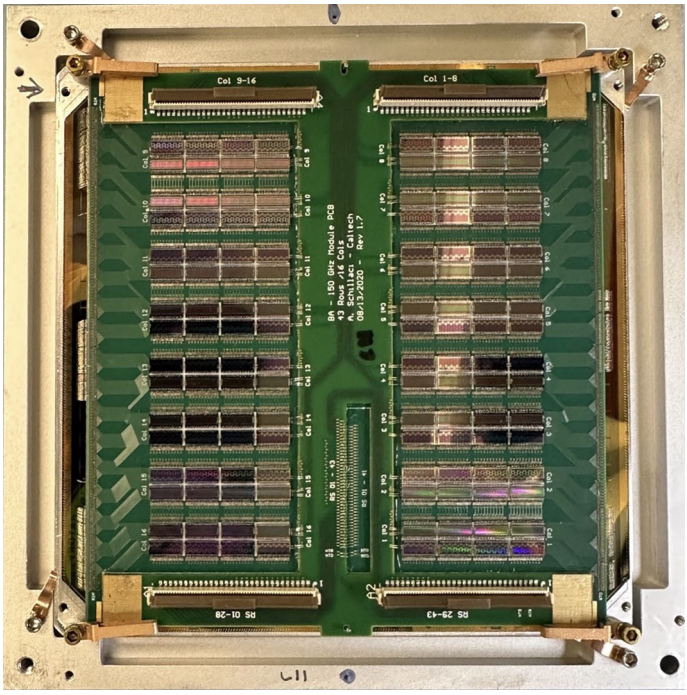

Fig. 3 A detector module with exposed MUX Nyquist PCB, fully populated with SQUID chips. The picture shows the high density of lines that are routed from the chips to the sides of the PCB. The number of wire bonds is equally large. The PCB in the picture is about 6 inches in diagonal

3 Warm Readout Electronics

The multiplexing is controlled at room temperature by the MCE [6], based on a modular architecture, where four different kind of cards are in charge of different operations. The number of cards and MDM connectors in one MCE subrack varies, and the required MCE version depends on the size of the array that needs to be read out. For the BICEP Array 30/40GHz receiver, a standard MCE subrack is used. A standard MCE includes one clock card, three bias cards and either two or four readout cards.

For the BICEP Array 150GHz receiver, which incorporates ~ 8000 TESs in the focal plane, a mechanical redesign was required to double the number of detectors that a single MCE can read out. The DMCE includes two clock cards, two address cards, eight readout cards and six bias cards. The signal is routed through ten 100 pins MDM connectors and to two bus backplanes and two instrument backplanes (see Fig. 4). The MDM connectors are encapsuled in aluminum enclosures called filter boxes. In order to increase the linear density of connectors, in the new version of the MCEs, we rotated the filter boxes of 90 degrees with respect to the filter rail. Making the filter rail shorter than the rest of the subrack was necessary in order to fit the necessary 3 DMCE subracks on the bottom of the cryostat [Fig. 1].

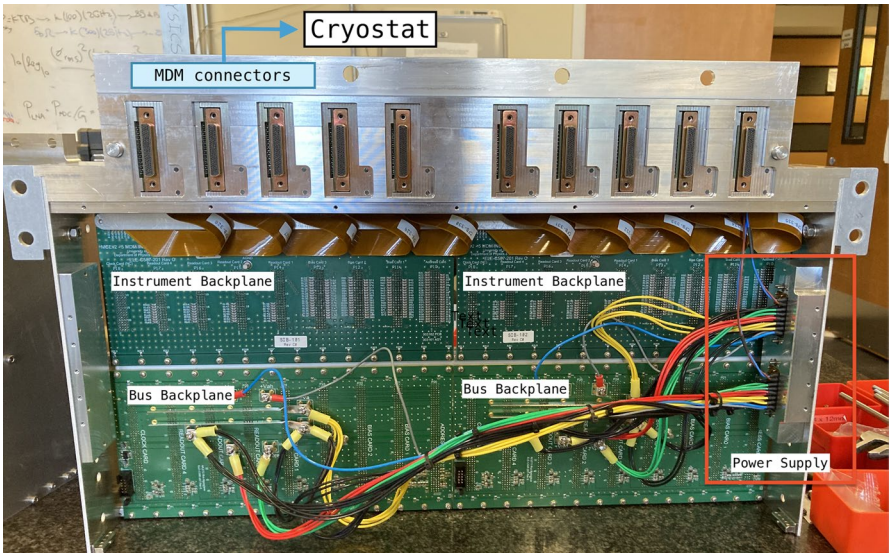

Fig. 4 DMCE side which mates to the cryostat. The back cover is removed in this picture. The filter boxes are inserted in a one piece aluminum block called filter rail, which is aligned to the cryostat through two alignment pins. MDM connectors can be translated in the direction orthogonal to this page turning a set of shafts, accessible from the opposite DMCE side with a torque wrench

The flexes that carry the signal from the MDM connector to the backplanes are longer than in the previous version and need to be installed turning them in a specific twisted S shape before mating them to the 100 pins Hirose connectors on the backplane. The two bus backplanes are powered independently by two power connectors. The two power connectors are assembled together in an aluminum cassette and can be mounted on either side panel of the subrack. In the DMCE, the fans are automatically powered by these same harness that powers the backplanes, and are turned on whenever the power it is connected.

The mating between each DMCE subrack and the cryostat is done at the bottom of the cryostat, through a double density feedthrough flange. The two alignment dowel pins at the extreme ends of the filter rail are mated to a pin and a slot on the feedthrough flange side. In order for the mating to be successful, the two pieces of each flange need to be aligned with high precision. To make sure that this is the case, an alignment tool was built. The alignment tool is a single long piece of metal that grabs the two half flanges' pin holes and keeps the flanges aligned while they get mounted to the cryostat.

Finally, the DMCE is attached to the cryostat through a long mounting flange located on top of the filter rail and two mounting ears per side. A DMCE can read out a matrix of 41 rows x 64 columns.

DMCEs come from a mostly mechanical redesign of the standard MCE subrack, where we have not only made the crate smaller but also optimized the shape to fit a set of three crates on a single cryostat. The DMCE backplane schematics are similar to the previous version, with small changes in the signal assignment. A further

reduction in size would not be possible without a major electrical redesign and signal rerouting.

The DMCEs designed and built for the BA 150GHz receiver showed reliability and high performance.

4 Multiplexing Rate

The time that we spend on each row when multiplexing, which we call row length, needs to be tuned. Ideally we want to multiplex as fast as we can (i.e., making the length of each row visit to be as short as possible), so as to limit the contribution to total noise from SQUID aliased noise. However, in practice the multiplexing rate is limited by the SQUID settling time. Measurements of the SQUID settling time are acquired as part of the readout characterization process. The goal is to acquire a direct measurement of the minimum time interval the electronics need to spend on each. This parameter is extracted as the time that it takes for the SQ1 to go back within some threshold of its final offset value, after which we established the SQUID converges quickly to the final offset we are reading out. This data set is acquired sampling at a frequency of $f_{\text{samp}} = 50MHz$.

For the BICEP Array 150GHz receiver, measurements of the settling time show that we can set the length of the row visit as short as $\sim 1\mu s$ (see Figs. 5 and 6).

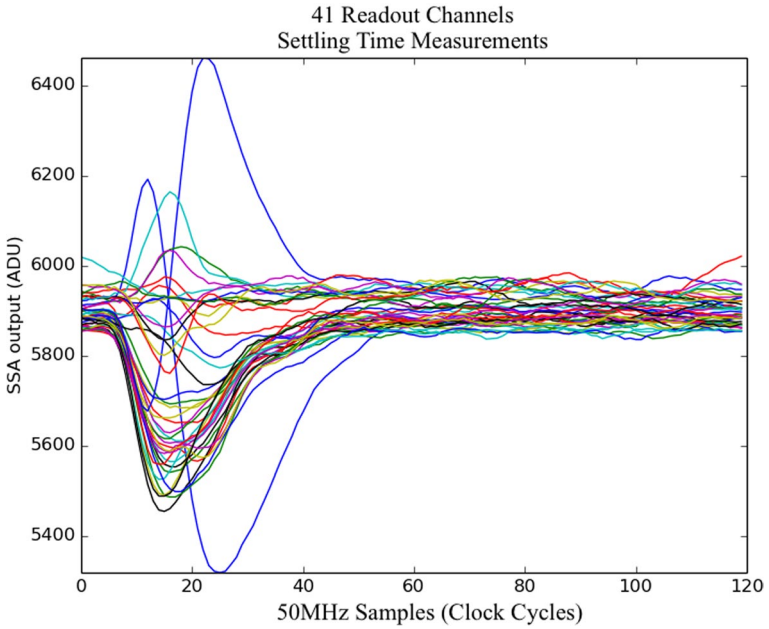

Fig. 5 Time streams showing the SQUID behavior after switching to a new row, on the BA 150 GHz receiver. These measurements were acquired as part of the BICEP Array 150GHz receiver readout characterization. This plot shows time streams for all rows on one column overlapped. The data set was acquired at a sampling frequency of $f_{\text{samp}} = 50MHz$, switching between rows every 120 clock cycles

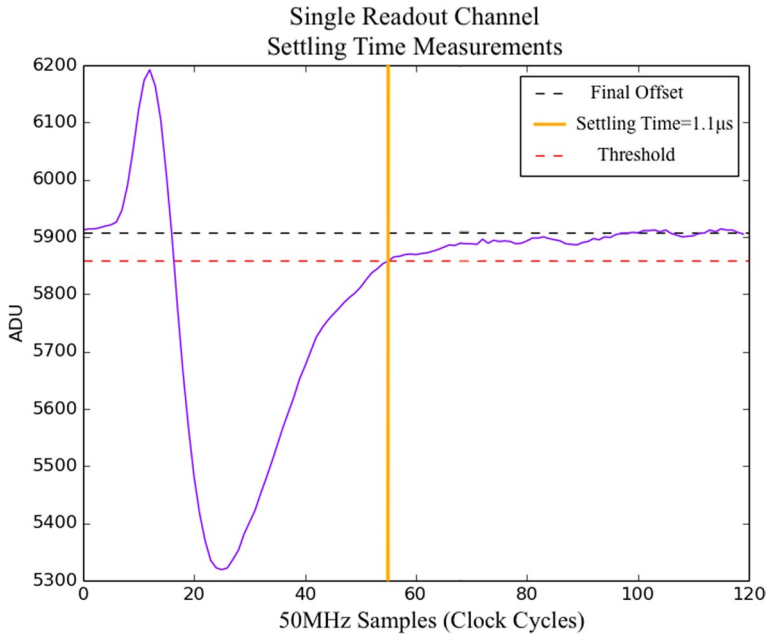

Fig. 6 A single time stream for one row in the column (that is one SQUID+TES pair) picked from the ensemble in Fig. 5. Here is plotted the final offset level, the threshold used to extract the settling time ($offset \pm 50ADU$) and the resulting settling time for this single readout channel

Additionally, for higher-frequency receivers the number of rows we want to multiplex (MUX factor) is higher (see Tab.1). In the BICEP Array 30/40GHz receiver, we multiplex 33 rows, while in the 150GHz receiver we multiplex 41 rows.

The multiplexing rate is given by MUX rate = switch rate / number of rows, where the switch rate is the frequency at which we switch between rows when multiplexing. If the number of multiplexed rows increases at constant switch rate, our mux rate decreases and we pay a noise penalty from introducing extra aliased noise into our data set.

As a matter of fact, we measured the 90th percentile of the SQUID settling time to be $1.3\mu s$(65 clock cycles) in the BA 150GHz receiver and $2\mu s$ (100 clock cycles) in the BA 30/40GHz receiver. By increasing the switching rate accordingly, we measured a $\sim$ 10% improvement in noise equivalent temperature (NET) in the BA 150GHz receiver (see Fig. 7). This data set has been acquired by the fielded BA 150GHz receiver on sky.

5 Conclusion

Time-domain multiplexing is a mature and well-characterized technology, with a noise performance that is suitable for high-demanding applications aiming to set tight cosmological constraints[2]. In all BICEP/Keck telescopes, MCEs have

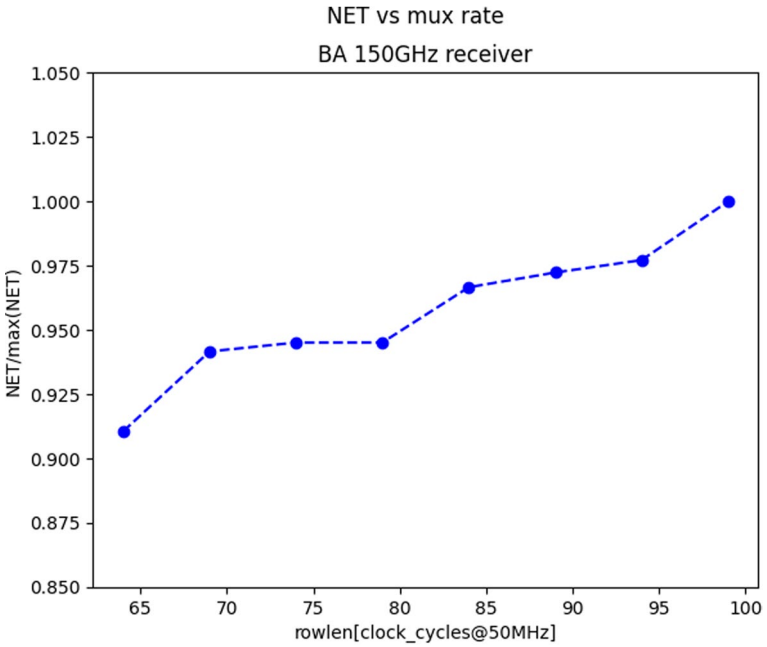

Fig. 7 Noise equivalent temperature (NET) as a function of switching rate, normalized to the value with a $2\mu s$ switching rate (100 clock cycles at 50MHz). As a function of the number of clock cycles, we wait when switching rows. This data set was acquired with the fielded BICEP Array 150GHz receiver. This data set shows that pushing down the row length from 100 to 65 results in a $\sim 9\%$ improvement in NET

been in charge of the time-domain multiplexing. The detector density in the BICEP Array high-frequency receivers required a redesign of the readout electronics to double the number of channels that a single subrack can read out. The double MCEs have been deployed to the south pole and used to characterize the readout performance of the BICEP Array 150GHz receiver. For the BA 150GHz receiver, we were able to increase our multiplexing rate by 35%, which resulted in a 9% improvement in the detector NETs.

Acknowledgements BICEP/Keck Array project have been made possible through a series of grants from the National Science Foundation and by the Keck Foundation. The development of antenna-coupled detector technology was supported by the JPL Research and Technology Development Fund and NASA Grants. The development and testing of focal planes were supported by the Gordon and Betty Moore Foundation at Caltech. Readout electronics were supported by a Canada Foundation for Innovation grant to UBC. The computations in this paper were run on the Odyssey cluster supported by the FAS Science Division Research Computing Group at Harvard University. We thank the staff of the US Antarctic Program and in particular the South Pole Station without whose help this research would not have been possible. Tireless administrative support was provided by Nancy Roth-Rappard.

Author Contributions SF wrote the main manuscript text, analyzed the data and made the figures. All the rest of the authors reviewed the manuscript and provided important feedback.

Declarations

Conflict of interest The authors declare no conflict of interest.

References

1. D.R. Barron et al., Conceptual design of the modular detector and readout system for the CMB-S4 survey experiment. Proc. SPIE Int. Soc. Opt. Eng. **12190**, 164 (2022). https://doi.org/10.1117/12.2630494
2. BICEP/Keck Collaboration. Improved constraints on primordial gravitational waves using planck, wmap, and bicep/keck observations through the 2018 observing season. Phys. Rev. Lett., **127**, 151301 (2021). https://doi.org/10.1103/PhysRevLett.127.151301
3. A. Schillaci et al., BICEP array: 150 GHz detector module development. J. Low Temp. Phys. (2023). https://doi.org/10.1007/s10909-023-03005-w
4. C. Zhang et al., Characterizing the sensitivity of 40 ghz tes bolometers for bicep array. J. Low Temp. Phys. **199**(3–4), 968–975 (2020). ISSN 1573-7357. https://doi.org/10.1007/s10909-020-02411-8
5. D.C. Goldfinger et al., End-to-end modeling of the TDM readout system for CMB-S4. J. Low Temp. Phys. (2023b)
6. E.S. Battistelli et al., Functional description of read-out electronics for time-domain multiplexed bolometers for millimeter and sub-millimeter astronomy. J. Low Temp. Phys. **151**(3), 908–914 (2008). https://doi.org/10.1007/s10909-008-9772-z
7. L. Moncelsi et al., Receiver development for BICEP Array, a next-generation CMB polarimeter at the South Pole. SPIE **11453**, 1145314 (2020). https://doi.org/10.1117/12.2561995
8. S. Fatigoni, Constraining the Inflationary Universe from the South Pole. PhD thesis, University of British Columbia (2023)
9. M. Hasselfield., Galaxy cluster cosmology with the Atacama Cosmology Telescope. PhD thesis, University of British Columbia (2013)

Authors and Affiliations

S. Fatigoni[1,15] · P. A. R. Ade[2] · Z. Ahmed[3,4] · M. Amiri[5] · D. Barkats[6] · R. Basu Thakur[1,8] · C. A. Bischoff[7] · D. Beck[4] · J. J. Bock[1,8] · V. Buza[6] · J. Cheshire[9] · J. Connors[6] · J. Cornelison[6] · M. Crumrine[9] · A. J. Cukierman[1] · E. V. Denison[13] · M. I. Dierickx[6] · L. Duband[10] · M. Eiben[6] · J. P. Filippini[11,12] · A. Fortes[4] · M. Gao[1] · C. Giannakopoulos[7] · N. Goeckner-Wald[4] · D. C. Goldfinger[3,4] · J. A. Grayson[4] · P. K. Grimes[6] · G. Hall[9] · G. Halal[4] · M. Halpern[5] · E. Hand[7] · S. A. Harrison[6] · S. Handerson[3,4] · S. R. Hildebrandt[1,8] · G. C. Hilton[13] · J. Hubmayr[13] · H. Hui[1] · K. D. Irwin[3,4] · J. H. Kang[4] · K. S. Karkare[4] · S. Kefeli[1] · J. M. Kovac[6] · C. L. Kuo[3,4] · K. Lau[1] · A. Lennox[11] · T. Liu[4] · K. G. Megerian[8] · O. Y. Miller[1] · L. Minutolo[1] · L. Moncelsi[1] · Y. Nakato[4] · H. T. Nguyen[8] · R. O'Brient[1,8] · S. Palladino[7] · M. A. Petroff[6] · A. Polish[6] · T. Prouve[10] · C. Pryke[9] · B. Racine[6] · C. D. Reintsema[13] · T. Romand[1] · M. Salatino[4] · A. Schillaci[1] · B. L. Schmitt[6] · B. Singari[9] ·

A. Soliman[8] · T. St.Germaine[6] · A. Steiger[1] · B. Steinbach[1] · R. Sudiwala[2] · K. L. Thompson[3,4] · C. Tsai[6] · C. Tucker[2] · A. D. Turner[8] · C. Umiltà[7] · C. Vèrges[6] · A. Wandui[1] · A. C. Weber[8] · D. V. Wiebe[5] · J. Willmert[9] · W. L. K. Wu[14] · E. Yang[4] · E. Young[4] · C. Yu[4] · L. Zeng[6] · C. Zhang[1] · S. Zhang[1]

✉ S. Fatigoni
sofiaf@caltech.edu

[1] Department of Physics, California Institute of Technology, Pasadena, CA 91125, USA

[2] School of Physics and Astronomy, Cardiff University, Cardiff CF24 3AA, UK

[3] Kavli Institute for Particle Astrophysics and Cosmology, SLAC National Accelerator Laboratory, 2575 Sand Hill Rd, Menlo Park, CA 94025, USA

[4] Department of Physics, Stanford University, Stanford, CA 94305, USA

[5] Department of Physics and Astronomy, University of British Columbia, Vancouver, BC V6T1Z1, Canada

[6] Center for Astrophysics, Harvard and Smithsonian, Cambridge, MA 02138, USA

[7] Department of Physics, University of Cincinnati, Cincinnati, OH 45221, USA

[8] Jet Propulsion Laboratory, Pasadena, CA 91109, USA

[9] Minnesota Institute for Astrophysics, University of Minnesota, Minneapolis, MN 55455, USA

[10] Service des Basses Temperatures, Commissariat al Energie Atomique, 38054 Grenoble, France

[11] Department of Physics, University of Illinois at Urbana-Champaign, Urbana, IL 61801, USA

[12] Department of Astronomy, University of Illinois at Urbana-Champaign, Urbana, IL 61801, USA

[13] Kavli Institute for Cosmological Physics, University of Chicago, Chicago, IL 60637, USA

[14] Department of Physics, Enrico Fermi Institute, University of Chicago, Chicago, IL 60637, USA

[15] National Institute of Standards and Technology, Boulder, CO 80305, USA